Vortex-Core Structure Observed with a Scanning Tunneling Microscope

H. F. Hess, R. B. Robinson, and J. V. Waszczak

AT&T Bell Laboratories, 600 Mountain Avenue, Murray Hill, New Jersey 07974

The superconducting-vortex-core spectra show a zero-bias peak which splits within a coherence length of the core. Further away from the core these split peaks merge gradually with the gap edge and give a direct local measure of the superfluid velocity. The vortex-core states are imaged at both the Fermi energy and just below the gap to reveal two different sixfold star-shaped structures. The anisotropy and size of these images may be a consequence of the crystalline band structure with its charge-density-wave gap as well as the interaction of the neighboring vortices of the Abrikosov flux lattice.

PACS numbers: 74.50.+r, 61.16.Di

The detailed structure of the superconducting vortex core has long been a topic of considerable theoretical interest.[1-3] With only a few exceptions,[4] a rigorous check of many assertions of microscopic vortex structure has remained beyond the scrutiny of experiment. The development of the scanning tunneling microscope (STM) with its ability to spatially resolve the local density of states with atomic resolution finally gave promise to a new experimental check. A recent STM experiment[5,6] revealed unexpected zero-bias peaks at the vortex core and revived theoretical interest[7-10] in this subject. These recent theories confirmed the existence of the zero-bias peak and some[8,10,11] also predicted that more structure in the local spectra near a vortex core should be visible at sufficiently low temperatures.

In this Letter we report the existence of several features in the vortex structure. The theoretically predicted[8,10,11] evolution of the spectra on approaching a vortex core is clearly confirmed. Far away from the core the energy of these spectral features can be interpreted to give local "velocity" measurements of the circulating superfluid current. Finally, we observe that these vortices are not simple cylindrically symmetric objects but instead have sixfold symmetry, probably reflecting the angular variation of the superconducting parameters and the underlying crystalline band structure.

The sample is 2H-NbSe$_2$, a layered crystal with a charge-density-wave (CDW) transition at 33 K. STM images show the angular orientation of the atomic lattice, CDW, and the flux lattice. STM spectra[6] show a fraction of the Fermi surface is removed by the CDW gap of 33 meV. The remainder of the Fermi surface undergoes a BCS transition at 7.2 K which has an in-plane coherence length[12] ξ of 77 Å and a penetration depth λ of 690 Å. The microscope was operated at 0.3 ± 0.1 K, with an improved energy resolution to 0.1 meV. Other details of the experimental procedure are described in Refs. 5 and 6.

Three spectral data sets are plotted in Fig. 1 in "VY" format. The grey scale is a measure of dI/dV (normalized to the metallic tunneling conductance) ranging from 0 corresponding to black to 2 corresponding to white. The horizontal voltage scale V consists of 64 equally spaced voltage points ranging from -2 to 2 mV. The vertical position scale Y corresponds to 128 positions on the surface along an 800-Å line. This line intersects a vortex at about 200 Å. Figure 1(a) was taken with a magnetic field of 500 G (vortex spacing ~ 2200 Å). The direction of the Y axis is 24° away from the crystallographic **a** direction. The angular orientation of the vortex lattice is always observed to be identical to the crystalline lattice. Figures 1(b) and 1(c) were taken with a field of 2000 G. In Fig. 1(b) the Y vector is rotated 30° from the **a** direction (in **k**$_{CDW}$ direction) and in Fig. 1(c)
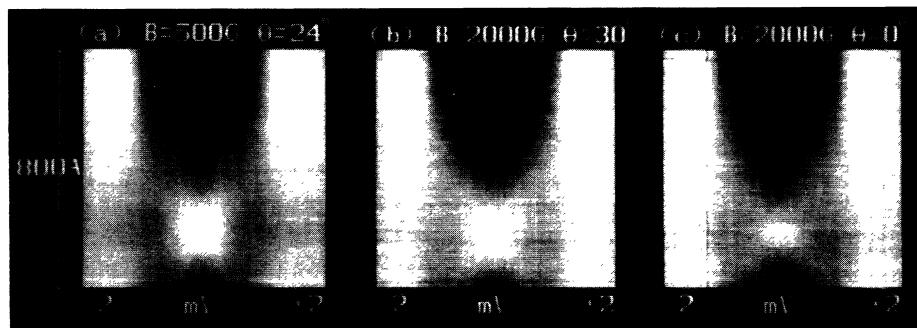

FIG. 1. VY scans displaying the evolution of the $dI/dV(V,Y)$ spectra on a grey scale as one moves through a core. The angle θ corresponds to the difference between the crystalline lattice vector **a** and the Y-scan direction.
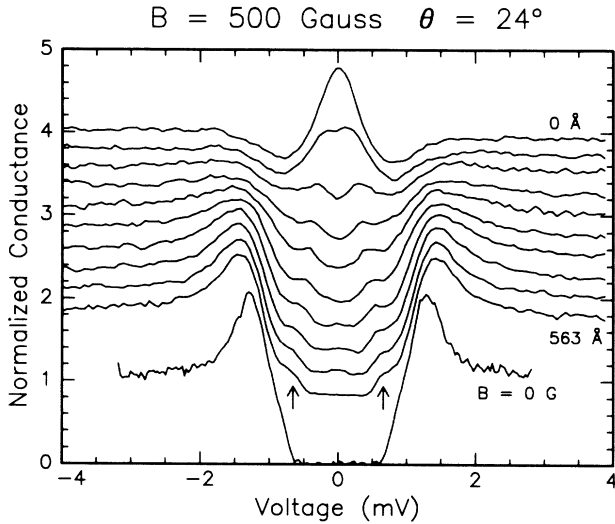
FIG. 2. Explicit dI/dV curves from the data set of Fig. 1(a). The normalized value of 1 corresponds to a metallic tunneling conductance of 5×10^{-9}. The 563-Å curve has been shifted up by 0.75 and successive ones are each shifted by 0.25 normalized unit of conductance. The bottom trace shows the spectra at zero magnetic field.
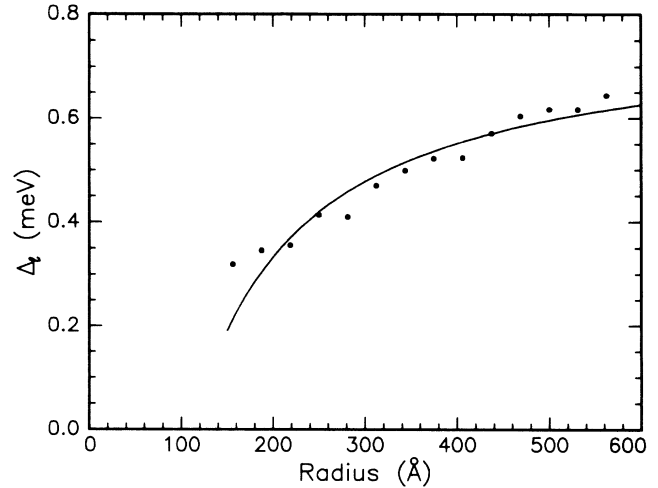

FIG. 3. Superfluid-velocity-induced energy shift from the data of Fig. 1(a). The solid curve gives a comparison to a superposition of cylindrically symmetric model vortices under identical conditions.

it is identical to the **a** direction.

In this representation the superconducting gap manifests itself as the dark vertical band in the center. The zero-bias peak of the vortex core is visible as the bright region at the bottom center of the picture. This peak is observed to split into higher-energy quasiparticle excitations (both above and below the Fermi level) as one samples spectra away from the core and forms an X structure inside the gaps of Fig. 1. The rate of splay of the two subgap peaks depends on magnetic field, splitting faster at higher fields so that the maximum splitting occurs at a point halfway between vortices, i.e., at ~ 1200, ~ 550, and ~ 630 Å from the core for Figs. 1(a), 1(b), and 1(c). The basic idea[8,10,11] is that the more energetic bound quasiparticle states have higher angular momentum and are located at larger radii so that the X structure reflects the relationship between most probable radius and energy. Sufficiently far away, these excitations become of order Δ, the superconducting gap, and merge with the quasiparticle excitations at the gap edge. We use the voltage of maximum local curvature $d^3I/dV^3(V,\mathbf{r})$ to indicate $\Delta_l(\mathbf{r})$. For example, Fig. 2 plots a few slices of the 500-G data set. The two vertical arrows indicate $\Delta_l(\mathbf{r})$ for the 563-Å curve. The resulting energy shifts of the peaks are shown in Fig. 3.

Well away from the vortex core the modification of the spectra can be understood in terms of a simple argument given by Cyrot.[3] If $r \gg \xi$ then $|\Delta(r)|$ is constant and only the superfluid current perturbs the spectra. It shifts the energy of a quasiparticle from its BCS value by $\mathbf{p}_f \cdot \mathbf{v}_s$. The strongest effect will occur for quasiparticles moving exactly up or downstream with the super-

fluid current $\mathbf{v}_s$. The lowest energy of the velocity-shifted states $\Delta_l(\mathbf{r})$ for one London equation vortex[1] is given by

$$\Delta_l(\mathbf{r}) = \Delta - \mathbf{p}_f \cdot \mathbf{v}_s(\mathbf{r}) = \Delta \left[1 - \frac{\pi}{2} \frac{\xi}{\lambda} K_1 \left(\frac{r}{\lambda} \right) \right].$$

$K_1(\ )$ is the imaginary Bessel function of order 1. The values of $\Delta = 0.7$ meV, $\xi = 77$ Å, and $\lambda = 690$ Å in this model produce the solid curve shown in Fig. 3. For higher magnetic fields a simple model of the velocity field can be constructed from a superposition of vortices based on the London equation. Not surprisingly, this would imply a minimum-energy shift at the Wigner-Seitz cell boundaries between vortices where $\mathbf{v}_s$ should vanish. The steeper velocity gradient is reflected in the more flattened X structures of Figs. 1(b) and 1(c).

The notion of cylindrical symmetry becomes questionable in light of the slight differences between Figs. 1(b) and 1(c). Further evidence that these vortices are not round but in fact star shaped is shown in Fig. 4. Both axes X and Y are spatial coordinates on the surface ranging over 1500 Å. The color scale measures $dI/dV(0$ mV) and $dI/dV(0.5$ mV) for vortices produced by a 500- and 2000-G field in units normalized to metallic conductance. The points of the 0.5-mV star are directed along the crystalline and Abrikosov lattice vector ($\theta = 0$), while the streamers of the 0-mV vortex are rotated by 30°, and go along the CDW direction.

A series of profiles of these vortex images is shown in Fig. 5. Data from 2000-G vortices are also plotted. The height of the 0-mV peak is somewhat suppressed by the higher magnetic field. This is in agreement with the general experimental trend observed in the 200–30000-G range. However, other variables (presumably dirt-
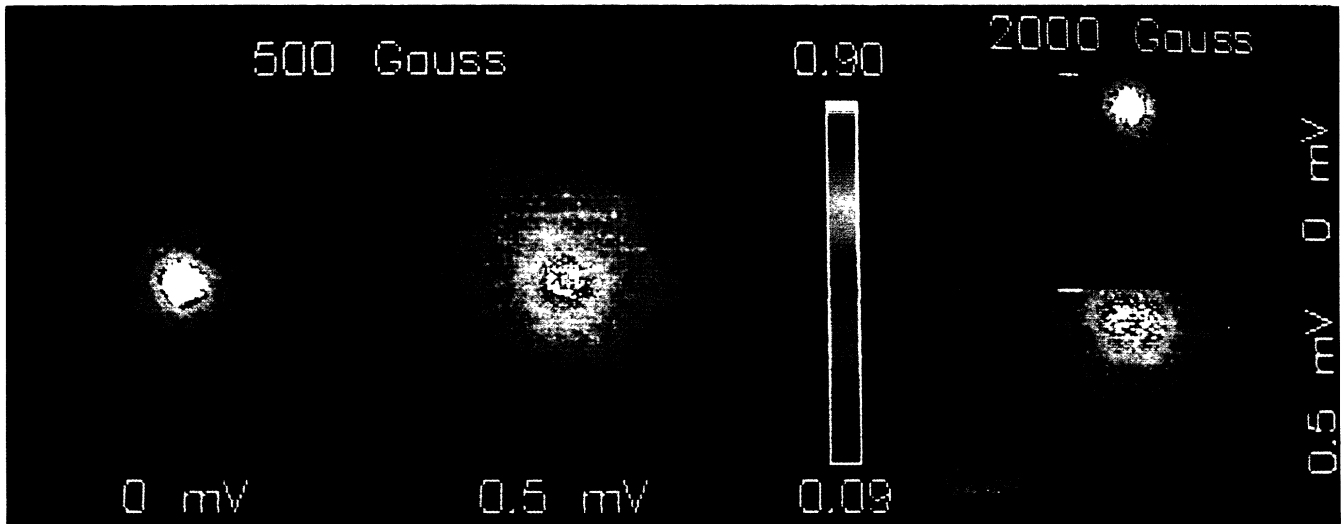
FIG. 4. Simultaneously taken XY images of $dI/dV(0$ mV,$x,y)$ and $dI/dV(0.5$ mV,$x,y)$ with $B = 500$ G and the same for 2000 G. The width of all images is 1500 Å. Differential tunneling conductance of 0.9 and larger in normalized units is shown as white.

induced effects) such as sample dependence and, to a certain extent, vortex location complicate this issue. The anisotropy is most evident in the amplitude in the tails where $r > 300$ Å. The amplitude of the 0-mV tail is larger in the 30° (streamer) direction (top two curves). For the 2000 G, $\theta = 30°$, and 0-mV data we find a local maximum in the conductance at $r \sim 700$ Å, indicated by the arrow. This corresponds roughly to a point in the center of the triangle of three neighboring vortices. The data suggest that a simple linear superposition of three intersecting streamers may explain this feature. Such an intercore region of enhanced conductance has been previously noted[6] at 10 kG. The 0.5-meV profiles are significantly broadened and lower in amplitude with a possible dip at the origin.
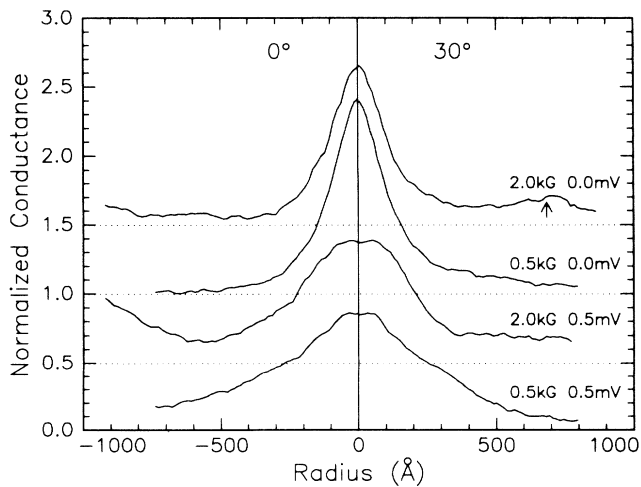
FIG. 5. Profiles of the vortices at 0° and 30° from the data of Fig. 4.

These images and their profiles can be interpreted as the wave-function density of the bound states within a few kT of the Fermi energy and 0.5 meV below it. The larger spatial extent of the 0.5-mV data with the slight dip at the origin is qualitatively consistent with the shape expected[8,10,11] for the larger angular momentum states. The size and the sixfold shape of the vortex is influenced by the hexagonal crystalline band structure as well as the Abrikosov flux lattice. The star pattern at large radius in the 0.5-mV data can be interpreted as constant-velocity contours. The outermost contour corresponds to the location where the gap is reduced to 0.5 meV. This suggests that the points of the stars have a strongly reduced gap and therefore the largest superfluid velocity. At 30° further the opposite is true and equivalently high velocities can be encountered only at a much smaller radius. Since the current $J(\theta) = e \cdot n_s(\theta) \cdot v_s(\theta)$ must be conserved (assuming negligible radial contributions), the angular variations in $v_s(\theta)$ may be a consequence of the angular variations in $n_s(\theta)$. In fact, the direction of highest v_s is observed to be identical to the CDW direction, where the CDW gap does reduce or eliminate the density of conducting states. At higher magnetic fields the overall v_s is reduced by the closer neighboring cores and a smaller but similar star-shaped image is observed.

The situation is different for the ground-state wave functions, since a proper interpretation must take into account the 30° orientational difference between it and the more energetic wave functions. A qualitative explanation of ground-state wave-function shape may lie in the angle-dependent coherence length. Since the radial decay length[6,13] of the ground state is $\pi\xi$, a diverging coherence length in the k_{CDW} direction could explain these images. The 30°-angle difference observed in Fig. 4 is then tied to the notion that the ground-state wave

functions are a superposition of mainly radially oriented and decaying quasiparticle plane-wave states, while the more energetic high angular momentum states observed just below the gap emphasize a local plane wave oriented in the θ direction.

The strong anisotropies may influence the zero-field tunneling spectra. These spectra (Fig. 2, lowest curve) appear to be quite different from a thermally broadened or lifetime smeared BCS form. The conductance increases almost linearly from 0 at 0.6 meV to a maximum at 1.3 meV before dropping off. This may well be consistent with a distribution of energy gaps. The weighting of this distribution is determined by the various tunneling probabilities into different parts of the Fermi surface. Whether this distribution can be deduced from the observed in-plane anisotropies or is a consequence of a possible in-plane 1.2-meV and out-of-plane 0.6-meV variation of the gap[14,15] has yet to be determined.

In conclusion, we have performed local spectroscopic measurements near a superconducting vortex with an improved energy resolution of $\Delta/10$. Near the core the zero-bias peak splits with increasing distance from the core as predicted by several recent calculations. Far away from the core the gap is reduced by the superfluid velocity. Images of the vortex as the Fermi energy and just below the gap show two different star structures. The anisotropy may reflect both angular-dependent superconducting parameters such as coherence length, density of states, or gap size, as well as the contribution of the superfluid velocity from neighboring cores.

[1]For a general review, see, e.g., A. L. Fetter and P. C. Hohenberg, in *Superconductivity,* edited by R. D. Parks (Marcel Dekker, New York, 1969), Vol. 2.

[2]C. Caroli, P. G. de Gennes, and J. Matricon, Phys. Lett. **9**, 307 (1964); C. Caroli and J. Matricon, Phys. Konden. Mater. **3**, 380 (1965).

[3]M. Cyrot, Phys. Konden. Mater. **3**, 374 (1965).

[4]H. W. Weber, J. Scheller, and G. Lippman, Phys. Status Solidi (b) **57**, 515 (1973).

[5]H. F. Hess *et al.,* Phys. Rev. Lett. **62**, 214 (1989).

[6]H. F. Hess *et al.,* J. Vac. Sci. Technol. A **8**, 450 (1990).

[7]A. W. Overhauser and L. L. Daemen, Phys. Rev. Lett. **62**, 1691 (1989); Phys. Rev. B **40**, 10778 (1989).

[8]J. D. Shore, M. Huang, A. T. Dorsey, and J. P. Sethna, Phys. Rev. Lett. **62**, 3089 (1989).

[9]F. Gygi and M. Schluter, Phys. Rev. B **41**, 822 (1990).

[10]U. Klein, Phys. Rev. B **41**, 4819 (1990).

[11]F. Gygi (private communication).

[12]P. de Trey, S. Gygax, and J. P. Jan, J. Low Temp. Phys. **11**, 421 (1973).

[13]J. D. Shore (private communication).

[14]B. P. Clayman, Can. J. Phys. **50**, 3193 (1972).

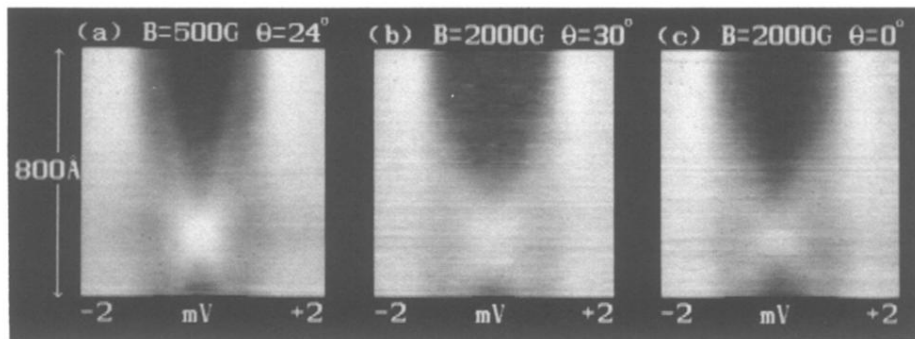[15]R. C. Morris and R. V. Coleman, Phys. Lett. **43A**, 11 (1973).

FIG. 1. *VY* scans displaying the evolution of the $dI/dV(V,Y)$ spectra on a grey scale as one moves through a core. The angle θ corresponds to the difference between the crystalline lattice vector **a** and the *Y*-scan direction.
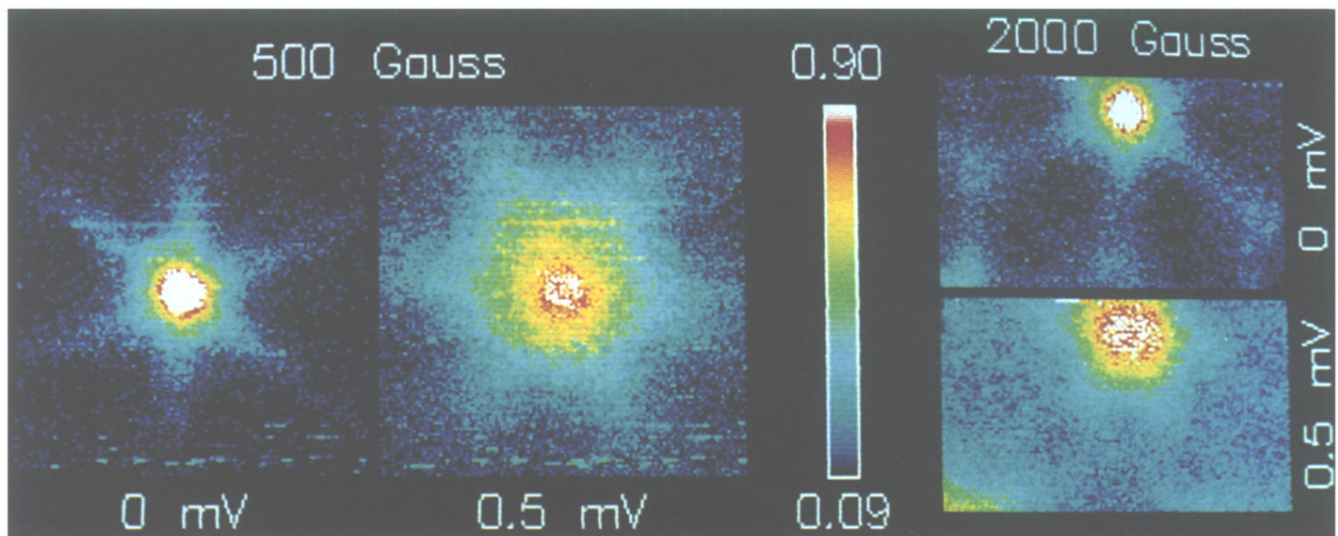
FIG. 4. Simultaneously taken *XY* images of $dI/dV(0$ mV$,x,y)$ and $dI/dV(0.5$ mV$,x,y)$ with $B = 500$ G and the same for 2000 G. The width of all images is 1500 Å. Differential tunneling conductance of 0.9 and larger in normalized units is shown as white.